nature photonics

ARTICLES

DOI: 10.1038/s41566-017-0006-2

Lasing in topological edge states of a one-dimensional lattice

P. St-Jean[1]*, V. Goblot[1], E. Galopin[1], A. Lemaître[1], T. Ozawa[2], L. Le Gratiet[1], I. Sagnes[1], J. Bloch[1] and A. Amo[1]

Topology describes properties that remain unaffected by smooth distortions. Its main hallmark is the emergence of edge states localized at the boundary between regions characterized by distinct topological invariants. Because their properties are inherited from the topology of the bulk, these edge states present a strong immunity to distortions of the underlying architecture. This feature offers new opportunities for robust trapping of light in nano- and micrometre-scale systems subject to fabrication imperfections and environmentally induced deformations. Here, we report lasing in such topological edge states of a one-dimensional lattice of polariton micropillars that implements an orbital version of the Su–Schrieffer–Heeger Hamiltonian. We further demonstrate that lasing in these states persists under local deformations of the lattice. These results open the way to the implementation of chiral lasers in systems with broken time-reversal symmetry and, when combined with polariton interactions, to the study of nonlinear phenomena in topological photonics.

Topological phase transitions in condensed matter have been studied extensively over the past decade. A key manifestation of these transitions is the emergence, at the frontier between materials exhibiting distinct topological phases, of localized states that are unaffected by disorder. One example of this topological protection is provided by chiral edge states at the surface of topological insulators that allow unidirectional transport immune to backscattering[1].

Initially proposed by Haldane and Raghu[2], the idea of extending topological arguments to the realm of photonics has recently triggered considerable efforts to engineer optical devices that are unaffected by local perturbations and fabrication defects[3]. For example, topological properties have been used to create polarization-dependent unidirectional waveguides[4], optical delay lines with enhanced transport properties[5], backscattering-immune chiral edge states[6–9] and protected bound states related to parity-time symmetry[10,11].

The emergence of edge states at the boundary between materials with distinct topological invariants provides an efficient way to create localized photonic modes whose existence is protected by topology[9]. Lasing in these kinds of modes would then be robust against fabrication defects, local deformations caused by temperature or other unstable ambient conditions and long-term degradation, all of which would otherwise result in the modification of the local optical potential[12]. The main difficulty that has prevented the observation of lasing in topological modes is the need to implement topological lattices in media exhibiting optical gain. In this sense, microcavity polaritons, mixed quasiparticules formed from the strong coupling between cavity photons and quantum well excitons[13], provide a unique platform: they allow for single-mode lasing in single micropillars[14], low-threshold lasing in planar structures[15,16]—even at room temperature[17,18]—and for the engineering of topological properties in lattices of resonators[19,20].

In this Article we report lasing in topological edge states of a one-dimensional lattice of coupled semiconductor micropillars. This lattice implements an orbital version of the Su–Schrieffer–Heeger (SSH) model by coupling $l=1$ polariton modes confined in a zigzag chain of micropillars. Under non-resonant optical pumping, we show that gain occurs in the topological states localized at the edges of the chain. Then, taking advantage of polariton interactions, we demonstrate the topological robustness of the lasing action against optically induced lattice deformations. These results open the way to the realization of topological lasers of arbitrary geometry, in which the lasing mode would be determined by the boundary between topologically distinct regions, regardless of its shape.

Orbital SSH model

To engineer topological edge states in a one-dimensional lattice, we implement an orbital version of the SSH model. The SSH model describes a one-dimensional lattice with two sites per unit cell and different intracell (t) and intercell (t') hopping amplitudes. Within the tight-binding approximation, such a model is captured by a Hamiltonian with chiral symmetry (Supplementary Section 1):

$$\hat{H}=\sum_j t\hat{a}_j\hat{b}_j^{\dagger}+t'\hat{a}_j^{\dagger}\hat{b}_j+h.c. \tag{1}$$

where $\hat{a}_j^{\dagger}$ ($\hat{b}_j^{\dagger}$) are the creation operators on the sublattice site a_j (b_j) in the jth unit cell. Its eigenstates form two bands ($\pm$) in momentum space separated by a gap of magnitude $2|t-t'|$. The eigenfunctions in the $\{a, b\}$ sublattice basis take the form[21] $|u_{k,\pm}\rangle=(1/\sqrt{2})(e^{-i\phi(k)},\pm 1)^{\dagger}$. $\hat{H}$ exhibits two topologically distinct phases associated with the two possible dimerizations $t>t'$ and $t<t'$. The different topology of these two phases is revealed by considering the winding $\mathcal{W}$ of phase $\varphi(k)$ across the Brillouin zone[21]:

$$\mathcal{W}=\frac{1}{2\pi}\int_{\mathrm{BZ}}\frac{\partial\phi(k)}{\partial k}\mathrm{d}k \tag{2}$$

which corresponds to the Zak phase divided by π.

Although the value of $\mathcal{W}$ associated with either dimerization depends on the definition of the unit cell, in finite-size chains the

[1]Centre de Nanosciences et de Nanotechnologies, CNRS, Université Paris-Sud, Université Paris-Saclay, C2N - Marcoussis, 91460 Marcoussis, France. [2]INO-CNR BEC Center and Dipartimento di Fisica, Università di Trento, I-38123 Povo, Italy. *e-mail: philippe.st-jean@c2n.upsaclay.fr

choice is unambiguous because t is defined by the hopping amplitude between the first and second sites of the chain. Under this definition, the $t > t'$ and $t < t'$ dimerizations exhibit respectively strong and weak coupling between the edge sites and the rest of the chain (depicted in Fig. 1a,d) and correspond to the trivial ($\mathcal{W} = 0$) and non-trivial ($\mathcal{W} = 1$) topological phases[21]. Band structures calculated for chains of 20 sites exhibiting $\mathcal{W} = 0$ and $\mathcal{W} = 1$ are presented in Fig. 1b and e, respectively. The most notable difference is the existence in the latter case of two states at the centre of the energy gap corresponding to topological states localized at each end of the chain. The distribution of the wavefunction over the first six sites, for the eigenstate indicated by the filled circle, is presented in the inset of Fig. 1e. Its envelope (dashed line) decays as λ^n, where n is the unit cell number counted from the edge and $\lambda = t/t'$.

To implement the SSH Hamiltonian, we consider the collective photon modes of a one-dimensional lattice of coupled polariton micropillars. The photonic modes of a single micropillar are confined in the three dimensions of space, leading to discrete energy levels: the ground state s exhibits a cylindrical symmetry along the growth axis, and the first excited states $p_{x,y}$ present two degenerate antisymmetric orbitals orthogonal to each other (Fig. 1h). The orbital version of the SSH model considered in this work relies on the coupling of these p orbitals in a one-dimensional lattice of micropillars arranged in a zigzag configuration (Fig. 1g).

In zigzag chains, p_x and p_y orbitals are respectively oriented along the diagonal and antidiagonal axes (Fig. 1c,f) and the hopping amplitude between consecutive micropillars strongly depends on the orientation of the axis linking these pillars. The coupling is typically an order of magnitude stronger for orbitals oriented along the hopping direction than for orbitals oriented perpendicular to the hopping[22]. We define these different hopping strengths as longitudinal (t_l) and transverse (t_t), respectively. Note that p_x and p_y form independent subspaces, as the 90° angles between diagonal and antidiagonal links of the chain prevent the coupling between adjacent orthogonal orbitals. Consequently, if we consider the subspace of p_x modes (Fig. 1c), photons are subject to an alternating hopping strength as we move along the chain. This corresponds exactly to the SSH model described in Hamiltonian (1), where the intra- and intercell hopping strength are respectively t_l and t_t. The large hopping anisotropy ($t_l \gg t_t$) leads to the opening of a significant energy gap, as depicted in Fig. 1b. This subspace exhibits strong coupling (t_l) between the first two (and last two) pillars and does not present edge states; on the other hand, the p_y subspace (Fig. 1e,f) starts and ends with the weak coupling t_t and contains a topological edge state at each end of the chain. Similar twofold subspaces have been studied using the polarization-dependent hopping of s modes in zigzag chains of photonic resonators[23,24].

Imaging orbital states in the linear regime

To implement this orbital SSH model, we etched zigzag chains of coupled micropillars from a planar microcavity containing 12 GaAs quantum wells sandwiched between two $Ga_{0.05}Al_{0.95}As/Ga_{0.8}Al_{0.2}As$ Bragg mirrors with 32 (top) and 40 (bottom) pairs (see Methods and ref. [25] for further details). We can probe the orbital states by exciting the system nonresonantly with a continuous-wave single-mode laser focused on an elliptical spot of 2 µm width and 50 µm length (full-width at half-maximum, FWHM) that covers 25 unit cells of the lattice (upper part of Fig. 2a). The photoluminescence spectra present an energy splitting between linear polarizations oriented along and perpendicular to the main axis of the chain[26]. For each of these two polarizations the system presents identical characteristics. We select the emission linearly polarized parallel to the long axis of the chain (similar results were obtained in the orthogonal polarization). All measurements presented in this work were performed at 4 K.

Figure 2a shows the photoluminescent intensity as a function of emission energy and momentum (directly proportional to the angle of emission) for low-power excitation (200 µW). It reveals three families of energy bands. The lowest band (S-band) arises from the coupling of s-mode polaritons. Due to their cylindrical symmetry, the hopping amplitude between these modes is completely isotropic ($t = t'$) and no energy gap is observed. At higher energies, we observe two sets of bands (P-bands) formed from the coupling of p modes. They are separated by an energy gap of 1.7 meV due to the orbital hopping anisotropy $t_l \gg t_t$. At even higher energies, additional bands arising from the coupling of d modes can be seen.

When moving the elliptical spot over the edge of the chain (Fig. 2b), we observe the emergence of a discrete state in the middle of the P-bands energy gap (indicated by blue circles), as expected for the topological edge states associated to the p_y subspace. Figure 2d dis-

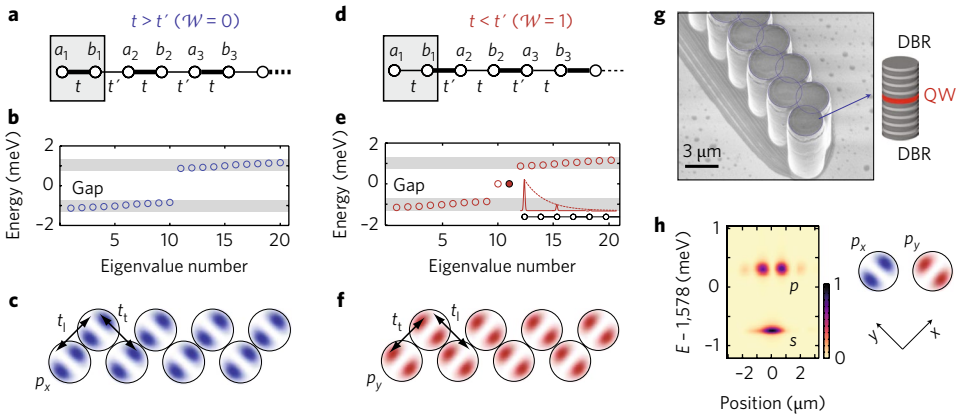

Fig. 1 | Tight-binding calculations of the orbital SSH Hamiltonian. a,**d**, Schematic representations of the two dimerizations in the SSH model. The unit cell is indicated by the grey rectangles. **b**,**e**, Band structure associated with both dimerizations. Grey areas represent the spectral position of the bands. Inset in **e**: distribution of the wavefunction (solid line) and of the envelope function (dashed line) over the first six sites of the lattice for the gap state indicated by the filled circle. **c**,**f**, Schematic representations of the p_x and the p_y subspaces. Each subspace exhibits a distinct dimerization determined by the orientation of the longitudinal (t_l) and transversal (t_t) couplings at the edge of the chain. **g**, SEM image of one end of a zigzag chain of coupled micropillars etched out of a cavity. The blue circles are added for visibility. The enlargement shows a schematic representation of a single pillar embedding quantum wells (QWs) between distributed Bragg reflectors (DBRs). **h**, Spectrally resolved real-space emission of an isolated micropillar showing s and p orbitals for polaritons (a schematic representation of the $p_{x,y}$ modes is presented on the right). E, emission energy.

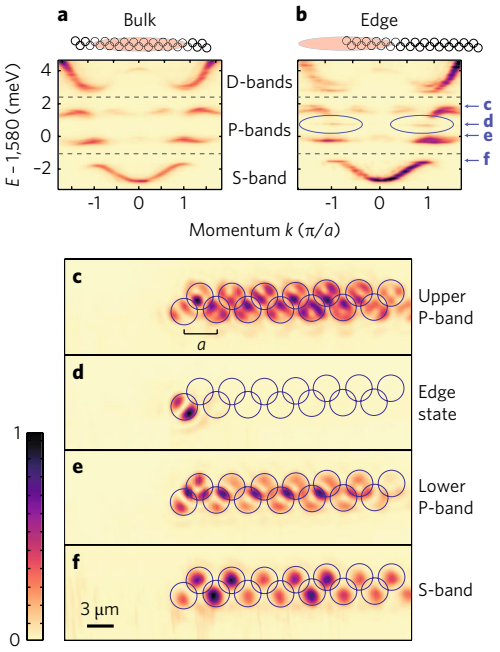

Fig. 2 | Momentum and real-space imaging of the polariton modes. **a**,**b**, Momentum space image of emission from the bulk (**a**) and edge (**b**) of a zigzag chain ($a = 3.4$ μm is the lattice periodicity, as depicted in **c**). E, emission energy. The area of the chain that is detected and excited is schematically represented on top of each figure. **c**–**f**, Spatial images of the photoluminescent intensity at the energies of the upper (**c**) and lower (**e**) P-bands, the S-band (**f**) and the orbital gap state (**d**). The excitation spot used for the spatial images is located over the edge of the chain, as depicted on top of **b**. Positions of the micropillars are indicated by blue circles. Blue arrows in **b** indicate the spectral position at which each image is taken.

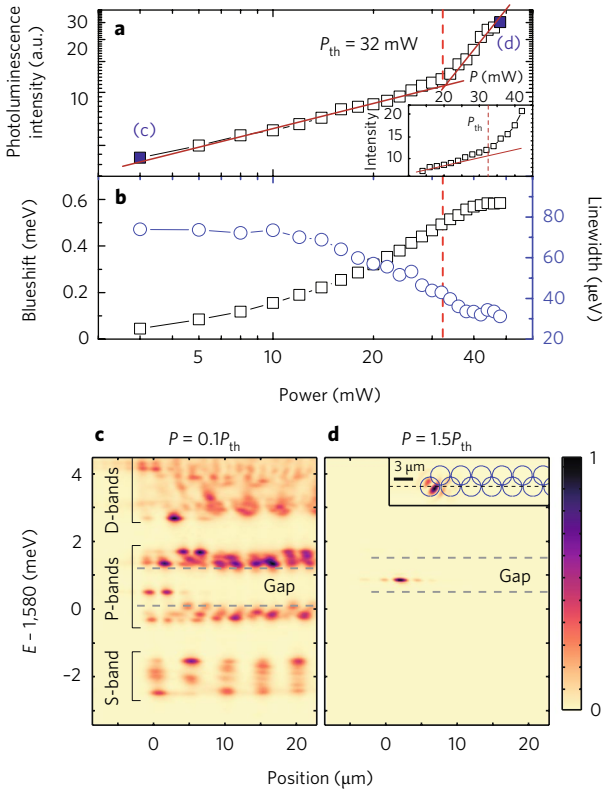

Fig. 3 | Emission in the lasing regime. **a**,**b**, Integrated intensity (**a**) and blueshift (**b**, black squares) and linewidth (**b**, blue circles) of the emission from the topological edge state as a function of excitation power. The lasing threshold is indicated by the dashed red line. Excitation is provided by an elongated spot centred over the edge of the chain, similar to that depicted in Fig. 2b. Inset in **a**: zoom-in of the threshold region on a linear-scale plot. **c**,**d**, Normalized photoluminescent intensity as a function of emission energy E and longitudinal position along the chain for an excitation power below (**c**) and above (**d**) the lasing threshold, corresponding to data points indicated by blue filled squares in **a**. The orbital bandgap is indicated by horizontal dashed lines. Inset in **d**: real-space image of the photoluminescence at the energy of the edge state (the position of the micropillars is indicated by blue circles and the dashed line shows the position at which the energy space cut in **d** is taken).

plays the real-space emission at the energy of this edge mode, attesting its strong localization at the end of the chain. An identical edge state (not shown here) is observed at the opposite end of the chain, as it also terminates with a weakly bound p_y mode. In contrast, the S- and P-bands exhibit emission over the whole excited area (Fig. 2c,e,f).

The gap-state wavefunction exhibits three features that unambiguously demonstrate its topological nature. First, we can see from the geometry of this edge state that it is formed from orbitals belonging to the topologically non-trivial p_y subspace. Secondly, we observe that this state is strongly localized in the last pillar: the intensity in the second unit cell is an order of magnitude weaker than in the first. This can be understood from the low ratio t_t/t_l, which sets the penetration depth of the topological edge state. From the measured size of the gap and amplitude of the bands, we estimate t_t/t_l to be 0.15, which is consistent with the observed localization in the outermost pillar. Finally, we observe at the energies of the upper and lower P-bands (Fig. 2c and e) that the wavefunction in the edge pillar only exhibits orbital modes belonging to the trivial subspace p_x. This is consistent with tight-binding calculations that show that the bulk states vanish at the edge pillars in the topologically non-trivial p_y subspace (Supplementary Section 2).

Lasing in the topological edge state

One interesting feature of polariton micropillars in the strong coupling regime is the ability to trigger lasing in excited states, such as the topological edge states described above. This is possible thanks to the driven-dissipative nature of cavity polaritons: the steady-state lasing is determined by the interplay of pumping intensity, polariton relaxation and emission lifetime[27–29]. Both the relaxation rate and the lifetime are strongly influenced by the photon–exciton detuning[30], that is, the energy difference between the bare photon and exciton modes that couple to form polaritons.

To achieve polariton lasing in the edge states of our orbital SSH chain, we select an exciton–photon detuning of −9.4 meV (see Methods), which favours relaxation of polaritons in the P-band states. Figure 3a presents the spatially integrated photoluminescence intensity at the energy of the edge state as a function of excitation power. A nonlinear increase in the intensity is observed at a threshold power of $P_{th} = 32$ mW, indicating the triggering of lasing in the topological edge state. Simultaneously, the linewidth of the emission collapses, evidencing the increase of temporal coherence characteristic of the lasing regime (blue circles in Fig. 3b). Energy-resolved real-space images (Fig. 3d) show that for $P = 1.5P_{th}$, the emission from the edge state completely overcomes that of the bulk bands (Supplementary Section 3). The three observed spots correspond to lobes of p_y orbitals in the first and third pillars. In the inset of Fig. 3d we see that the localization of the edge state is well preserved in the lasing regime.

Note that while interactions between polaritons in the lasing mode are negligible, these polaritons interact repulsively with a

highly populated exciton reservoir injected by the excitation laser and located at the bare exciton energy[14,31]. As the excitation power is increased, these interactions rigidly shift to higher energies the whole band structure under the excitation spot (Fig. 3c,d). A summary of the blueshift of the topological edge state is reported in Fig. 3b for all excitation powers.

The fact that the chain lases preferentially in the edge state rather than in the bulk P-bands states can be explained by the localized character of the former. Indeed, polaritons in band states can propagate away from the excitation spot, reducing their lifetime and precluding lasing in these states in favour of the confined edge state.

Robustness of the topological lasing

We now investigate the robustness of the topological lasing mode against local deformations of the lattice. The SSH Hamiltonian (equation (1)) presents a chiral symmetry, that is, it anticommutes with the σ_z Pauli matrix. The main consequence of this is that the topological modes appear in the middle of the gap. Because this symmetry is preserved when considering disorder in the hopping strengths (t, t'), the energy and localization of the topological modes are immune to this type of disorder (Supplementary Section 1). Therefore, the kind of local perturbations to which this mode is most sensitive are changes of on-site energies, which break the chiral symmetry, especially in the first lattice site, because the strong localization of the wavefunction (Fig. 2d) mitigates the effect of energy perturbations in other sites.

To evaluate theoretically the effect of such an energy perturbation in the first pillar, we add an on-site energy term $U_1 a_1^\dagger a_1$ in the Hamiltonian presented in equation (1) (Fig. 4a). By diagonalizing this perturbed Hamiltonian for a chain of 20 pillars, we can evaluate the evolution of the energy and wavefunction of the topological edge mode in the p_y subspace as a function of U_1 (we used $t_1 = 1$ meV and $t_t = 0.15$ meV, which reproduce the experimentally observed P-bands and gap). The main effect of the perturbation U_1 is to modify the energy of the edge mode in the gap, as depicted in Fig. 4b. Remarkably, its spatial localization is hardly affected: even for a perturbation energy $U_1 = 0.8$ meV, for which the edge state is almost resonant with the upper P-band, the wavefunction is strongly localized over the first pillar (Fig. 4d). This is further evidenced by the red line in Fig. 4f showing a high probability density of the edge state on the first pillar when varying U_1 from 0 up to 0.85 meV, at which point the edge state merges with the bulk band.

To experimentally test the robustness of lasing in the edge state against perturbations of the energy of the edge pillar, we use the interactions between polaritons and the exciton reservoir. The reservoir is populated by a non-resonant excitation and lies at the bare exciton energy, 11 meV above the lasing mode. Excitons in this reservoir interact repulsively with low-energy polaritons, inducing their blueshift with a magnitude controlled by the excitation power[14,31]. The inset of Fig. 4g shows the energy of the edge-state emission as a function of excitation power when using a small pump spot of 3.5 μm (FWHM) diameter localized on the first pillar. The injected exciton reservoir continuously increases the local energy of the first pillar, resulting in a blueshift of the lasing mode. In agreement with the simulations, the localization length is immune to the perturbation, as we observe that the emission remains highly confined in the first pillar over the whole power dependence (Fig. 4e, squares in Fig. 4f). One of the consequences of the robustness of the confinement is that the power density threshold for lasing remains the same for both the extended and localized excitation spots (~30 W cm^{-2}; see Supplementary Section 4 for the detailed lasing characteristics of the latter scheme). This behaviour is clear evidence of the robustness of the topological mode to local perturbations.

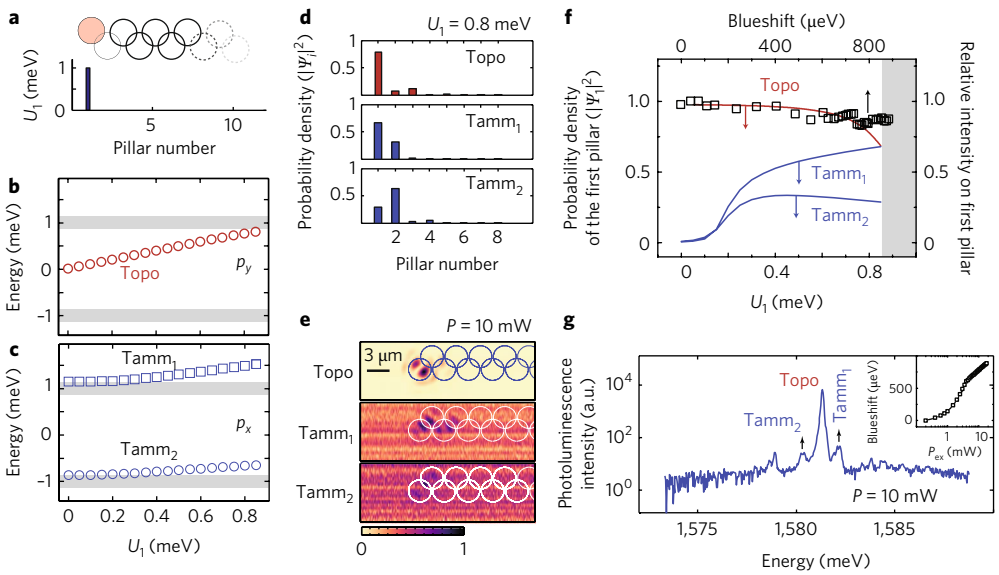

Fig. 4 | SSH Hamiltonian with broken chiral symmetry. a, Schematic representation of the distribution of on-site energies considered for the theoretical investigation of a localized perturbation. **b**,**c**, Calculated energies of topological (Topo in the p_y subspace) and non-topological (Tamm$_{1,2}$ in p_x) edge states of the locally perturbed SSH Hamiltonian, as a function of the on-site energy of the first pillar U_1. Grey areas indicate positions of the upper and lower P-bands. **d**, Squared amplitude of the calculated wavefunctions for the three edge states presented in **b** (Topo) and **c** (Tamm$_{1,2}$) for $U_1 = 0.8$ meV. **e**, Spatial distribution of the photoluminescence at the energies of Topo, Tamm$_1$ and Tamm$_2$ for an excitation localized over the edge pillar, with a power of $P = 3P_{th} = 10$ mW. The colour scale is identical to that used in Fig. 2. **f**, Calculated evolution of the localization (defined as the wavefunction squared amplitude at the first pillar) of the topological (Topo, red line) and non-topological (Tamm$_{1,2}$, blue lines) edge states as a function of perturbation energy U_1. Black squares present the measured relative intensities of the photoluminescence from Topo at the position of the first pillar as a function of its spectral blueshift. The position of the upper P-band is indicated by the grey area. **g**, Photoluminescence spectrum for the same excitation conditions as in **e**. Inset: evolution of the measured blueshift of the topological edge state as a function of excitation power.

In contrast, the topologically trivial p_x subspace presents a very different behaviour. Simulations of the perturbed Hamiltonian for the trivial dimerization show that the energy shift of the first pillar results in the emergence of two localized modes (labelled $\text{Tamm}_{1,2}$ in Fig. 4c) with energies in the central gap and above the upper P-band, respectively. They appear for $U_1 \neq 0$ and correspond to non-topological Tamm modes, which have been extensively discussed in the context of surface states induced by symmetry-breaking perturbations[32–34] (Supplementary Section 5). In contrast to the topological edge state, their wavefunction extends over a few pillars (Fig. 4d) and their distribution strongly varies with the value of U_1. This behaviour is visible in Fig. 4f, (blue lines), showing a low calculated weight of their wavefunction on the edge micropillar. Experimentally, they appear in the zigzag chain as a weak emission (peaks on both sides of the topological state in Fig. 4g). Their spatial distribution only contains p_x components and extends significantly further than the topological edge mode, as shown in Fig. 4e.

Note that despite the fact that the localized reservoir induces the emergence of Tamm modes in the p_x subspace of the zigzag chain, lasing takes place dominantly in the topological p_y edge mode over the explored power range. This is a consequence of the stronger localization of the topological mode, which overlaps more efficiently with the small pump spot than the Tamm modes and thus presents a lower lasing threshold. A fundamental difference between the topological and Tamm modes in the SSH chain is that the former appears as a single state in the gap, while the latter appear in pairs for $U_1 \neq 0$. In a lattice containing only the trivial dimerization, the Tamm states would then be prone to multimode effects[34].

Perspectives

The observation of lasing in a topologically protected edge state presented here provides a direct demonstration of robust light trapping in topological structures. Furthermore, by comparing the localization of topologically trivial and non-trivial modes, we have highlighted the immunity of the latter against local perturbations. These results open the way to lasing in modes with more complex geometries, for instance in kink-modes localized at the domain wall between chains with different windings[23]. The most exciting perspective of this work is to extend the results to two-dimensional lattices where we envision, in systems with broken time-reversal symmetry, one-dimensional topological lasers with arbitrary geometries[35] and channels allowing backscattering-immune transport of coherent light[36,37]. In addition, polariton interactions employed in the present work demonstrate the suitability of cavity polaritons for exploring nonlinear phenomena in topological photonics[38].

Methods

Methods, including statements of data availability and any associated accession codes and references, are available in the online version of this paper.

Received: 21 April 2017; Accepted: 20 July 2017;
Published online: 29 September 2017

References

1. Hasan, M. Z. & Kane, C. L. Colloquium: topological insulators. *Rev. Mod. Phys.* **82**, 3045–3067 (2010).
2. Haldane, F. D. M. & Raghu, S. Possible realization of directional optical waveguides in photonic crystals with broken time-reversal symmetry. *Phys. Rev. Lett.* **100**, 013904 (2008).
3. Lu, L., Joannopoulos, J. D. & Soljačić, M. Topological photonics. *Nat. Photon.* **8**, 821–829 (2014).
4. Söllner, I. et al. Deterministic photonemitter coupling in chiral photonic circuits. *Nat. Nanotech.* **10**, 775–778 (2015).
5. Mittal, S. et al. Topologically robust transport of photons in a synthetic gauge field. *Phys. Rev. Lett.* **113**, 087403 (2014).
6. Wang, Z., Chong, Y., Joannopoulos, J. D. & Soljačić, M. Observation of unidirectional backscattering-immune topological electromagnetic states. *Nature* **461**, 772–775 (2009).
7. Hafezi, M., Demler, E. A., Lukin, M. D. & Taylor, J. M. Robust optical delay lines with topological protection. *Nat. Phys.* **7**, 907–912 (2011).
8. Hafezi, M., Mittal, S., Fan, J., Migdall, A. & Taylor, J. M. Imaging topological edge states in silicon photonics. *Nat. Photon.* **7**, 1001–1005 (2013).
9. Rechtsman, M. C. et al. Photonic Floquet topological insulators. *Nature* **496**, 196–200 (2013).
10. Weimann, S. et al. Topologically protected bound states in photonic paritytime-symmetric crystals. *Nat. Mater.* **16**, 433–438 (2017).
11. Poli, C., Bellec, M., Kuhl, U., Mortessagne, F. & Schomerus, H. Selective enhancement of topologically induced interface states in a dielectric resonator chain. *Nat. Commun.* **6**, 6710 (2015).
12. Pilozzi, L. & Conti, C. Topological lasing in resonant photonic structures. *Phys. Rev. B* **93**, 195317 (2016).
13. Carusotto, I. & Ciuti, C. Quantum fluids of light. *Rev. Mod. Phys.* **85**, 299–366 (2013).
14. Bajoni, D. et al. Polariton laser using single micropillar GaAs–GaAlAs semiconductor cavities. *Phys. Rev. Lett.* **100**, 047401 (2008).
15. Deng, H., Weihs, G., Santori, C., Bloch, J. & Yamamoto, Y. Condensation of semiconductor microcavity exciton polaritons. *Science* **298**, 199–202 (2002).
16. Kasprzak, J. et al. Bose–Einstein condensation of exciton polaritons. *Nature* **443**, 409–414 (2006).
17. Christopoulos, S. et al. Room-temperature polariton lasing in semiconductor microcavities. *Phys. Rev. Lett.* **98**, 126405 (2007).
18. Kéna-Cohen, S. & Forrest, S. R. Room-temperature polariton lasing in an organic single-crystal microcavity. *Nat. Photon.* **4**, 371–375 (2010).
19. Milićević, M. et al. Orbital edge states in a photonic honeycomb lattice. *Phys. Rev. Lett.* **118**, 107403 (2017).
20. Baboux, F. et al. Measuring topological invariants from generalized edge states in polaritonic quasicrystals. *Phys. Rev. B* **95**, 161114 (2017).
21. Delplace, P., Ullmo, D. & Montambaux, G. Zak phase and the existence of edge states in graphene. *Phys. Rev. B* **84**, 195452 (2011).
22. Jacqmin, T. et al. Direct observation of Dirac cones and a flatband in a honeycomb lattice for polaritons. *Phys. Rev. Lett.* **112**, 116402 (2014).
23. Solnyshkov, D., Nalitov, A. & Malpuech, G. Kibble–Zurek mechanism in topologically nontrivial zigzag chains of polariton micropillars. *Phys. Rev. Lett.* **116**, 046402 (2016).
24. Kruk, S. et al. Edge states and topological phase transitions in chains of dielectric nanoparticles. *Small* **13**, 1603190 (2017).
25. Sala, V. et al. Spin–orbit coupling for photons and polaritons in microstructures. *Phys. Rev. X* **5**, 011034 (2015).
26. Sturm, C. et al. All-optical phase modulation in a cavity-polariton Mach–Zehnder interferometer. *Nat. Commun.* **5**, 3278 (2014).
27. Richard, M. et al. Experimental evidence for nonequilibrium Bose condensation of exciton polaritons. *Phys. Rev. B* **72**, 201301 (2005).
28. Wouters, M., Carusotto, I. & Ciuti, C. Spatial and spectral shape of inhomogeneous nonequilibrium exciton–polariton condensates. *Phys. Rev. B* **77**, 115340 (2008).
29. Baboux, F. et al. Bosonic condensation and disorder-induced localization in a flat band. *Phys. Rev. Lett.* **116**, 066402 (2016).
30. Levrat, J. et al. Condensation phase diagram of cavity polaritons in GaN-based microcavities: experiment and theory. *Phys. Rev. B* **81**, 125305 (2010).
31. Wertz, E. et al. Spontaneous formation and optical manipulation of extended polariton condensates. *Nat. Phys.* **6**, 860–864 (2010).
32. Zak, J. Symmetry criterion for surface states in solids. *Phys. Rev. B* **32**, 2218–2226 (1985).
33. Malkova, N., Hromada, I., Wang, X., Bryant, G. & Chen, Z. Transition between Tamm-like and Shockley-like surface states in optically induced photonic superlattices. *Phys. Rev. A* **80**, 043806 (2009).
34. Blanco-Redondo, A. et al. Topological optical waveguiding in silicon and the transition between topological and trivial defect states. *Phys. Rev. Lett.* **116**, 163901 (2016).
35. Harari, G. et al. in *Conference on Lasers and Electro-Optics*, FM3A.3 (OSA, Washington, DC, 2016).
36. Nalitov, A., Solnyshkov, D. & Malpuech, G. Polariton Z topological insulator. *Phys. Rev. Lett.* **114**, 116401 (2015).
37. Karzig, T., Bardyn, C.-E., Lindner, N. H. & Refael, G. Topological polaritons. *Phys. Rev. X* **5**, 031001 (2015).
38. Hadad, Y., Khanikaev, A. B. & Alù, A. Self-induced topological transitions and edge states supported by nonlinear staggered potentials. *Phys. Rev. B* **93**, 155112 (2016).

Acknowledgements

The authors thank M. Milicevic and G. Montambaux for discussions. This work was supported by the French National Research Agency (ANR) project Quantum Fluids of Light (ANR-16-CE30-0021) and program Labex NanoSaclay via the project ICQOQS (grant no. ANR-10-LABX-0035), the French RENATECH network, the ERC

grant Honeypol and the EU-FET Proactive grant AQUS (project no. 640800). P.S.-J. acknowledges financial support from the Natural Sciences and Engineering Research Council of Canada (NSERC).

Author contributions

P.S.-J. performed the experiments with help from V.G., carried out the calculations, analysed the data and wrote the manuscript, with the guidance of J.B. and A.A. T.O. provided critical inputs to the theoretical analysis. E.G., A.L., L.L. and I.S. grew and processed the sample. J.B. and A.A. designed the sample and supervised the work. All authors revised the manuscript.

Competing interests

The authors declare no competing financial interests.

Additional information

Supplementary information is available for this paper at doi:10.1038/s41566-017-0006-2.

Reprints and permissions information is available at www.nature.com/reprints.

Correspondence and requests for materials should be addressed to P.S.-J.

Publisher's note: Springer Nature remains neutral with regard to jurisdictional claims in published maps and institutional affiliations.

Methods

Sample description. The zigzag chain of coupled micropillars was etched out of a planar semiconductor cavity with high quality factor ($Q \sim 72{,}000$) consisting of a $Ga_{0.05}Al_{0.95}As$ $\lambda/2$ layer embedded between two $Ga_{0.05}Al_{0.95}As/Ga_{0.2}Al_{0.8}As$ Bragg mirrors formed from 28 (40) pairs in the top (bottom) mirror. Three sets of four GaAs quantum wells of 7 nm width were grown at the three central maxima of the electromagnetic field in the cavity, resulting in strong photon–exciton coupling, exhibiting a 15 meV Rabi splitting. After the epitaxy, the cavity was processed by electron-beam lithography and dry etching to form a zigzag chain of overlapping cylindrical micropillars. The diameter of the pillars (3 μm) overcomes the centre-to-centre distance (2.4 μm), allowing for the hopping of polaritons[39]. The distance between consecutive pillars was constant and the orientation of the axis linking pillars alternated between +45° and −45° with respect to the length of the chain; these orientations were defined by axes $\hat{x}$ and $\hat{y}$, respectively (Fig. 1h).

An exciton photon detuning of $\delta = -9.4$ meV was chosen to favour lasing in P-bands. This detuning is defined as $\delta = E_c(0) - E_X(0)$, where $E_c(k)$ and $E_X(k)$ describe, respectively, the energy dispersion of S-mode cavity photons and quantum well excitons as a function of their in-plane momentum k.

Experimental technique. Non-resonant photoluminescence measurements were realized with a single-mode continuous-wave (c.w.) laser at 754 nm. The elongated spot was engineered using a cylindrical lens. The emission was collected through a microscope objective and imaged on the entrance slit of a spectrometer coupled to a charge-coupled device (CCD) camera with a spectral resolution of ~30 μeV. Real- and momentum-space photoluminescence images were realized by imaging the sample surface and the Fourier plane of the objective, respectively. A $\lambda/2$ waveplate and a polarizer were used to select emission polarized either along or across the long axis of the chains. The sample was cooled to $T = 4$ K. Schematic diagrams of the experimental set-up are provided in Supplementary Section 6.

Data availability. The data that support the plots within this paper and other findings of this study are available from the corresponding author upon request.

References

39. Galbiati, M. et al. Polariton condensation in photonic molecules. *Phys. Rev. Lett.* **108**, 126403 (2012).